

Continuous-variable quantum cryptography with an untrusted relay: Detailed security analysis of the symmetric configuration

Carlo Ottaviani,* Gaetana Spedalieri, Samuel L. Braunstein, and Stefano Pirandola†
Department of Computer Science, University of York, York YO10 5GH, United Kingdom

(Dated: December 7, 2024)

We consider the continuous-variable protocol of Pirandola *et al.* [arXiv.1312.4104] where the secret-key is established by the measurement of an untrusted relay. In this network protocol, two authorized parties are connected to an untrusted relay by insecure quantum links. Secret correlations are generated by a continuous-variable Bell detection performed on incoming coherent states. In the present work we provide a detailed study of the symmetric configuration, where the relay is midway between the parties. We analyze symmetric eavesdropping strategies against the quantum links explicitly showing that, at fixed transmissivity and thermal noise, two-mode coherent attacks are optimal, manifestly outperforming one-mode collective attacks based on independent entangling cloners. Such an advantage is shown both in terms of security threshold and secret-key rate.

PACS numbers: 03.67.Dd, 03.65.-w, 42.50.-p, 89.70.Cf

I. INTRODUCTION

Rather than layers of physical security or obscure coding in the distribution of a classical key [1], quantum cryptography claims to rely on the fundamental laws of quantum physics to provide secure quantum key distribution (QKD) [2]. In the simplest scheme, information is encoded on non-orthogonal states which are transmitted from Alice to Bob via a quantum channel. After classical procedures of error correction and privacy amplification, Alice and Bob are then able to distill shared secret bits [2]. Any attempt by Eve at gleaning information inevitably introduces noise in the quantum channel; by quantifying this noise, Alice and Bob determine how much distillation must be applied to make Eve's information negligible or if there is too much noise (breaching the *security threshold*) they abort the protocol.

Over the last several decades, QKD has been implemented many times, more recently even in simple network configurations [3–5]. By utilizing an iterated point-to-point strategy, a secret key may be shared with legitimate users on more distant network nodes. This strategy explicitly requires secure and trusted intermediate relay stations. However, modern communication protocols (e.g., TCP/IP) rely on a more advanced ‘end-to-end principle’ [6, 7] with simple, unreliable and untrusted relays; any layers of security are provided by the two end-parties.

A first step in this direction has been done by Ref. [8], which extended QKD to the mediation of an untrusted relay, void of quantum sources (e.g., entanglement) and performing a quantum measurement which generates secret correlations in remote stations. This idea of a measurement-based untrusted relay (also known as ‘measurement-device independence’) has been experi-

mentally implemented with discrete variables [9, 10].

More recently, the use of measurement-based untrusted relays has been introduced in continuous-variable QKD [11] with the aim of exploiting the advantages of bosonic systems [12, 13] in terms of cheap quantum sources and highly-efficient detectors. Indeed this protocol is able to achieve secret-key rates orders of magnitude higher than any protocol based on discrete-variable systems. This is possible thanks to the use of the cheapest possible quantum sources, i.e., coherent states, combined with simple linear optics and homodyne detectors at the relay station. Ref. [11] found that the optimal performances are achieved in the asymmetric configuration where the relay is close to one of the parties.

In this paper, we deepen the analysis of Ref. [11] considering the symmetric configuration where the relay is midway between Alice and Bob. Despite the fact this is not the optimal setup in terms of rates and security distances, it is still very important to analyze for potential applications in network scenarios where two parties are roughly equidistant from a public server or access point. Another reason for analyzing this kind of setup is in its simple analytical formulas for the secret-key rates. Using these formulas, we can provide a very detailed comparison between the most important Gaussian attacks against the quantum links.

In our cryptanalysis of the symmetric protocol we clearly show that, at fixed transmissivity and thermal noise on the links, the optimal eavesdropping strategy is a two-mode coherent Gaussian attack, where Eve injects quantum correlations in both the quantum channels leading to the relay. In this attack, these channels are combined (via beam-splitters) with two entangled modes, which have been prepared in a suitable Einstein-Podolsky-Rosen (EPR) state. Such a strategy greatly outperforms the single-mode collective attack based on two independent entangling cloners which was assumed in some recent investigations [16–18]. Any such security analysis relying on independent attacks on the channels is therefore incomplete and opens security loopholes.

*Electronic address: Carlo.Ottaviani@york.ac.uk

†Electronic address: Stefano.Pirandola@york.ac.uk

The paper is organized as follows: In Section II we describe the setup in the symmetric scenario. In Section III we analyze its security and provide a formula for the key rate. In Section IV we compare the various Gaussian attacks, identifying the optimal attack and the corresponding minimum key rate of the protocol. Finally, in Section V we draw our conclusions.

II. THE PROTOCOL

Let us consider the scenario where Alice and Bob do not access a direct communication link. Instead they connect to a perfectly-in-the-middle relay via insecure quantum links, as shown in Fig. 1(a). The relay is untrusted, meaning that it is assumed to be operated by Eve in the worst case scenario.

The protocol proceeds as follows: Alice and Bob possess two modes, A and B , which are prepared in coherent states, $|\alpha\rangle$ and $|\beta\rangle$, with randomly-modulated amplitudes (according to a complex Gaussian distribution with large variance). They send these modes to the intermediate relay where the output modes, A' and B' , are subject to a continuous-variable Bell detection [19]. This means that A' and B' are mixed on a balanced beam splitter and the output ports are conjugately homodyned: One port is homodyned in the \hat{q} -quadrature with outcome q_- , while the other port is homodyned in the \hat{p} -quadrature with outcome p_+ . Compactly, the measurement provides the complex outcome $\gamma := (q_- + ip_+)/\sqrt{2}$ which is then broadcast over a public channel.

To understand the working mechanism of the relay, first suppose there is no loss and noise in the links. In such a case, we have $\gamma \simeq \alpha - \beta^*$, so that the communication of γ creates *a posteriori* correlations between Alice's and Bob's variables. Each party can easily infer the variable of the other. For instance, Alice could compute the quantity $\alpha - \gamma \simeq \beta^*$ recovering Bob's encoding β up to detection noise [11]. This procedure partly recalls the post-processing of the two-way QKD protocols [20, 21].

Note that Eve's knowledge of variable γ would be of no help to extract information on the individual variables α and β , i.e., we have $I(\alpha : \gamma) = I(\beta : \gamma) = 0$ in terms of mutual information [22, 23]. By contrast, as a result of the broadcast of γ , the conditional mutual information of Alice and Bob becomes non-zero $I(\alpha : \beta | \gamma) > I(\alpha : \beta)$. Thus, if Eve wants to steal information, she needs to introduce loss and noise.

In general, the action of Eve may involve a global unitary operation correlating all the uses of the protocols. However, using random permutations of their data [25, 26], Alice and Bob can always reduce this scenario to an attack which is coherent within the single use of protocol. This can be a joint attack of both the links and the relay. The parties can further reduce this eavesdropping to consider a coherent attack of the links only, assuming a properly-working relay, i.e., a relay implementing a continuous-variable Bell detection. In par-

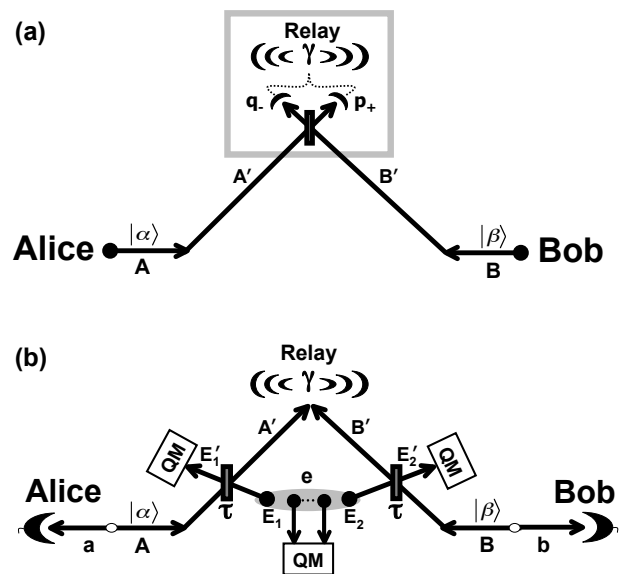


FIG. 1: (Color online) (a) Relay-based protocol performed in the symmetric configuration with the untrusted relay perfectly in the middle between the parties. Alice and Bob prepare coherent states with Gaussianly-modulated amplitudes, α and β , respectively. The relay performs a continuous-variable Bell measurement with complex outcome $\gamma := (q_- + ip_+)/\sqrt{2}$, which is publicly broadcast. From the knowledge of γ each party can infer the variable of the other party. (b) Entanglement-based representation of the protocol under two-mode Gaussian attack. Using two beam splitters with transmissivity τ , Eve injects ancillary modes, E_1 and E_2 , prepared in a two-mode Gaussian state with zero mean and CM in the symmetric normal form of Eq. (2). See text for details.

ticular, since the protocol is based on the Gaussian modulation and Gaussian detection of Gaussian states, the optimal coherent attack of the links will be based on a Gaussian unitary interaction [13–15]. See Ref. [11] for more details about this general reduction of the attack.

III. CRYPTOANALYSIS OF THE PROTOCOL

According to the previous discussion, we can reduce the attack to a two-mode Gaussian attack against the quantum links of Alice and Bob. The most realistic implementation of such an attack consists of two beam splitters combining the signals with ancillary modes prepared in a generally quantum-correlated Gaussian state (more exotic Gaussian attacks may be constructed using other canonical forms [27]). In particular, we will consider the symmetric configuration of this attack, where the parameters are identical for the two links, so that the performances of the protocol are invariant under exchange of Alice and Bob. In order to analyze this symmetric Gaussian attack, we adopt the entanglement-based (EB) representation of the protocol, where Alice's and Bob's ensembles of coherent states are simulated using two EPR

states subject to local heterodyne detections.

A. Entangled-based representation

The EB-representation of the protocol is described in Fig. 1(b). Alice and Bob possess two EPR states, ρ_{aA} and ρ_{bB} , with the same covariance matrix (CM) [13]

$$\mathbf{V}(\mu) = \begin{pmatrix} \mu\mathbf{I} & \sqrt{\mu^2 - 1}\mathbf{Z} \\ \sqrt{\mu^2 - 1}\mathbf{Z} & \mu\mathbf{I} \end{pmatrix}, \quad (1)$$

where $\mathbf{I} = \text{diag}(1, 1)$, $\mathbf{Z} = \text{diag}(1, -1)$ and $\mu \geq 1$.

By applying heterodyne detections to the remote modes, a and b , Alice and Bob prepares coherent states, $|\alpha\rangle$ and $|\beta\rangle$, on the other EPR modes, A and B , respectively. In particular, their amplitudes, α and β , are modulated according to a complex Gaussian distribution with variance $\varphi := \mu - 1$, that we take to be very large $\varphi \gg 1$. Modes A and B are then sent to the relay for detection.

B. Symmetric two-mode Gaussian eavesdropping

Alice's and Bob's modes A and B are mixed with ancillary modes, E_1 and E_2 , respectively. This is done by means of two beam-splitters with the same transmissivity τ . The ancillas belong to an environmental set $\{E_1, E_2, \mathbf{e}\}$ in the hands of Eve, and the reduced state of E_1 and E_2 is a zero-mean Gaussian state $\sigma_{E_1 E_2}$ with CM in the symmetric normal form

$$\mathbf{V}_{E_1 E_2} = \begin{pmatrix} \omega\mathbf{I} & \mathbf{G} \\ \mathbf{G} & \omega\mathbf{I} \end{pmatrix}, \quad \mathbf{G} := \begin{pmatrix} g & 0 \\ 0 & g' \end{pmatrix}. \quad (2)$$

Here ω is the variance of the thermal noise injected in the beam splitters, while \mathbf{G} accounts for the quantum correlations between the two ancillas. (The various parameters ω , g , and g' satisfy simple physical constraints imposed by the uncertainty principle [28, 29]).

The output modes, A' and B' , are subject to the continuous-variable Bell detection (with the outcome broadcast), while Eve's output modes, E'_1 and E'_2 , together with all the other ancillary modes \mathbf{e} are stored in a quantum memory, which is detected by an optimal coherent measurement at the end of the protocol.

Note that we may consider different transmissivities, τ_A and τ_B , for the beam splitters, and an asymmetric CM with different thermal variances, ω_A and ω_B . This is the general asymmetric case considered in Ref. [11]. However, when the relay is midway between the two parties, the amount of loss and noise present in the links is realistically expected to be identical. In other words, it is reasonable to consider here a symmetric attack as the one previously described, which has

$$\tau_A = \tau_B := \tau, \quad \omega_A = \omega_B := \omega. \quad (3)$$

Thanks to this symmetry, we can reduce the number of parameters and derive a simple analytical expression for

the secret-key rate, which allows us to perform a detailed analysis of the various specific symmetric attacks which are possible against our protocol. In particular, we can easily study the performances of these attacks in terms of the correlation parameters, g and g' , and identify the optimal one which minimizes key rate and security threshold. Furthermore, due to the symmetry, Alice and Bob can be interchanged, which implies that there is no difference between direct and reverse reconciliation [13]. In other words, we can consider a unique secret-key rate for the protocol (assuming one-way classical communication for error correction and privacy amplification).

C. Secret-key rate

Without loss of generality, we assume that Alice is the encoder of information (variable α) while Bob is the decoder, so that he post-processes his variable β to infer α . In the EB-representation, these variables are informationally equivalent to the outcomes of the heterodyne detections [11]. To derive the rate, we note that the Bell detection at the relay and the heterodyne detections of the two parties commute with each other. For this reason, we can equivalently compute the rate from the conditional state $\rho_{ab|\gamma}$ of modes a and b after the communication of the outcome γ . The rate is given by [11]

$$R = I_{ab|\gamma} - I_{E|\gamma}, \quad (4)$$

where $I_{ab|\gamma}$ is Alice and Bob's conditional mutual information, while $I_{E|\gamma}$ is Eve's Holevo information [23] on Alice's variable (which can be computed from the state of the output ancillas).

Since all output modes are in a global pure state and the various detections are rank-1, we can write [11]

$$I_{E|\gamma} = S(\rho_{ab|\gamma}) - S(\rho_{b|\gamma\alpha}), \quad (5)$$

where $S(\cdot)$ is the von Neumann entropy [23], computed on the post-relay state $\rho_{ab|\gamma}$ of Alice and Bob, and the double-conditional state $\rho_{b|\gamma\alpha}$ of Bob, conditioned to relay's and Alice's detections (computable from $\rho_{ab|\gamma}$).

D. Computation of the key rate

Both the mutual information $I_{ab|\gamma}$ and Eve's Holevo entropy $I_{E|\gamma}$ can be computed from the post-relay state $\rho_{ab|\gamma}$, in particular, from its CM $\mathbf{V}_{ab|\gamma}$. Imposing the symmetry conditions of Eq. (3) in the general expression of $\mathbf{V}_{ab|\gamma}$ computed in Ref. [11], we derive

$$\mathbf{V}_{ab|\gamma} = \begin{pmatrix} \mu\mathbf{I} & \mathbf{0} \\ \mathbf{0} & \mu\mathbf{I} \end{pmatrix} - \frac{\tau(\mu^2 - 1)}{2} \times \begin{pmatrix} \frac{1}{\tau\mu + \lambda} & & -\frac{1}{\tau\mu + \lambda} & \\ & \frac{1}{\tau\mu + \lambda'} & & \frac{1}{\tau\mu + \lambda'} \\ -\frac{1}{\tau\mu + \lambda} & & \frac{1}{\tau\mu + \lambda} & \\ & \frac{1}{\tau\mu + \lambda'} & & \frac{1}{\tau\mu + \lambda'} \end{pmatrix}, \quad (6)$$

where

$$\lambda := (1 - \tau)(\omega - g), \quad \lambda' := (1 - \tau)(\omega + g'). \quad (7)$$

Note that Eq. (6) represents a particular case of the general CM of Eq. (A10), which is obtained in the Appendix, where non-unit quantum efficiencies of the detectors are also included.

Now, we can easily compute [13] the symplectic spectrum of eq.(6) in the limit of large modulation $\mu \gg 1$, obtaining

$$\nu_1 \rightarrow \sqrt{\frac{\lambda\mu}{\tau}}, \nu_2 \rightarrow \sqrt{\frac{\lambda'\mu}{\tau}}. \quad (8)$$

Then, entropy term $S(\rho_{ab|\gamma})$ in Eq. (5) can be computed using the function

$$h(x) := \frac{x+1}{2} \log_2 \frac{x+1}{2} - \frac{x-1}{2} \log_2 \frac{x-1}{2} \quad (9)$$

$$\rightarrow \log \frac{e}{2} x + O\left(\frac{1}{x}\right) \quad \text{for } x \gg 1. \quad (10)$$

Thus, we have

$$S(\rho_{ab|\gamma}) = h(\nu_1) + h(\nu_2) \rightarrow \log \frac{e^2}{4\tau} \sqrt{\lambda\lambda'}\mu. \quad (11)$$

To compute $S(\rho_{b|\gamma\alpha})$ we derive the double-conditional CM $\mathbf{V}_{b|\gamma\alpha}$. We put Eq. (6) in the block-form

$$\mathbf{V}_{ab|\gamma} = \begin{pmatrix} \mathbf{A} & \mathbf{C} \\ \mathbf{C}^T & \mathbf{B} \end{pmatrix}, \quad (12)$$

and we apply a partial gaussian heterodyne measurement on Alice's remote mode a , given by [13, 19, 24],

$$\mathbf{V}_{b|\gamma\alpha} = \mathbf{B} - \mathbf{C}^T (\mathbf{A} + \mathbf{I})^{-1} \mathbf{C}, \quad (13)$$

which gives

$$\mathbf{V}_{b|\gamma\alpha} = \begin{pmatrix} \mu - \frac{(\mu^2-1)\tau}{\tau(\mu+1)+2\lambda} & 0 \\ 0 & \mu - \frac{(\mu^2-1)\tau}{\tau(\mu+1)+2\lambda'} \end{pmatrix}. \quad (14)$$

For $\mu \gg 1$, its symplectic eigenvalue is given by

$$\nu \rightarrow \frac{\sqrt{(\tau+2\lambda)(\tau+2\lambda')}}{\tau}, \quad (15)$$

and we have $S(\rho_{b|\gamma\alpha}) = h(\nu)$. We can then compute Eve's Holevo information, asymptotically given by

$$I_{E|\gamma} = \log_2 \frac{e^2 \sqrt{\lambda\lambda'}\mu}{4\tau} - h \left[\frac{\sqrt{(\tau+2\lambda)(\tau+2\lambda')}}{\tau} \right]. \quad (16)$$

Alice and Bob's conditional mutual information $I_{ab|\gamma}$ can be computed from the classical CM $\mathbf{V}(\alpha, \beta|\gamma) = (\mathbf{V}_{ab|\gamma} + \mathbf{I})/2$ describing their outcomes. After simple algebra, we get the asymptotic expression

$$I_{AB|\gamma} = \log_2 \frac{\tau\mu}{4\sqrt{(\tau+\lambda)(\tau+\lambda')}}. \quad (17)$$

As a result, we computed the following asymptotic secret-key rate for the symmetric Gaussian attack

$$R_{sym} = \log_2 \left[\frac{\tau^2}{e^2 \sqrt{\lambda\lambda'(\tau+\lambda)(\tau+\lambda')}} \right] + h \left[\frac{\sqrt{(\tau+2\lambda)(\tau+2\lambda')}}{\tau} \right], \quad (18)$$

which is function of the parameters τ , ω , g and g' .

A complete analysis of the performances of the scheme in presence of non-ideal experimental conditions is described in Appendix A

IV. DETAILED ANALYSIS OF THE SYMMETRIC ATTACKS

For fixed transmissivity τ and thermal noise ω affecting each link, there are remaining degrees of freedom in the two-mode Gaussian attack. These are given by the correlation parameters g and g' , which can be represented as a point on a 'correlation plane' (see Fig. 2). Each point of this plane describes an attack (with different amount and kind of correlations) to which it corresponds a specific key rate according to Eq. (18). Here we provide a detailed comparison between these attacks, showing how the optimal coherent attack greatly outperforms the collective attack based on independent entangling cloners.

Because of the symmetry, we have a simple characterization of the set of possible Gaussian attacks which are accessible to Eve. These correspond to points (g, g') such that [28, 29]

$$|g| < \omega, \quad |g'| < \omega, \quad (19)$$

$$\omega |g + g'| \leq \omega^2 + gg' - 1. \quad (20)$$

Among all these accessible attacks, those satisfying the further condition

$$\omega^2 - gg' - 1 \geq \omega |g - g'| \quad (21)$$

are separable attacks ($\sigma_{E_1 E_2}$ separable), while those violating Eq. (21) are entangled attacks ($\sigma_{E_1 E_2}$ entangled). See Fig. 2 for a numerical representation. In particular, we can identify the following attacks:

Collective attack. This is the simplest attack, represented by point (1) in Fig. 2, i.e., the origin of the plane ($g = g' = 0$). This corresponds to using two identical and independent entangling cloners with transmissivity τ and thermal noise ω . In fact, we have $\sigma_{E_1 E_2} = \sigma_{E_1} \otimes \sigma_{E_2}$, where σ_{E_k} ($k = 1, 2$) is a thermal state with variance ω , whose purification $\Phi_{E_k e_k}$ is an EPR state in the hands of Eve.

Separable attacks. Within the separable attacks we can identify points (2), (3), and (4) in Fig. 2. These are characterized by the condition $|g| = |g'| = \omega - 1$ and represent the separable attacks with the highest correlations. In particular, points (2) correspond to the cases

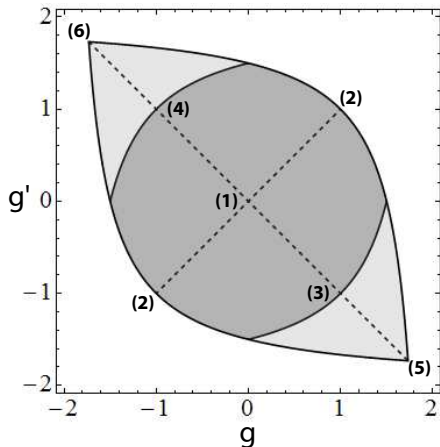


FIG. 2: (Color online) Correlation plan for a symmetric Gaussian attack. Given τ and ω (here set to 2), the attack is fully specified by the two correlation parameters (g, g') , whose accessible values are represented by the non-white area. In particular, the inner darker region represents the set of separable attacks ($\sigma_{E_1 E_2}$ separable), while the two outer and lighter regions represent entangled attacks ($\sigma_{E_1 E_2}$ entangled). The numbered points represent the specific attacks described in Sec. IV.

$g = g' = \omega - 1$ or $g = g' = 1 - \omega$, point (3) corresponds to $g = -g' = \omega - 1$, and point (4) to $g = -g' = 1 - \omega$.

EPR attacks. Finally, points (5) and (6) in Fig. 2 are the most entangled attacks, where Eve's ancillas E_1 and E_2 are described by an EPR state. Point (5) is the 'positive EPR attack' with $g = -g' = \sqrt{\omega^2 - 1}$, while (6) is the 'negative EPR attack' with $g = -g' = -\sqrt{\omega^2 - 1}$. The latter turns out to be the optimal attack against the protocol.

We now compare the performances of the previous attacks in Figs. 3 and 4. In Fig. 3 we fix the transmissivity $\tau = 0.9$ and we study the corresponding rates R as function of the thermal noise ω . In Fig. 4 we plot the security thresholds. These are given by the condition $R = 0$, and they are expressed in terms of maximum tolerable thermal noise versus transmissivity $\omega = \omega(\tau)$.

Our analysis identifies "good" and "bad" entanglement for the security of the protocol. Good entanglement refers to the entangled attacks in the bottom right area of Fig. 2, with $g = -g' > 0$, of which the attacks (3) and (5) are border points. This entanglement is good because it injects correlations of the type $\hat{q}_{E_1} \approx \hat{q}_{E_2}$ and $\hat{p}_{E_1} \approx -\hat{p}_{E_2}$, therefore helping the Bell detection (which projects on $\hat{q}_{A'} \approx \hat{q}_{B'}$ and $\hat{p}_{A'} \approx -\hat{p}_{B'}$). As a result, Eve actively helps the key distribution.

This is evident from the performance of the positive EPR attack (5) both in terms of rate (Fig. 3) and security threshold (Fig. 4). In fact, from Fig. 3, we see that the rate is *increasing* in the thermal noise ω and, in Fig. 4, we see a peculiar inversion of the security threshold so that thermal noise *above* the threshold is tolerable. These features are typical of all entangled attacks with

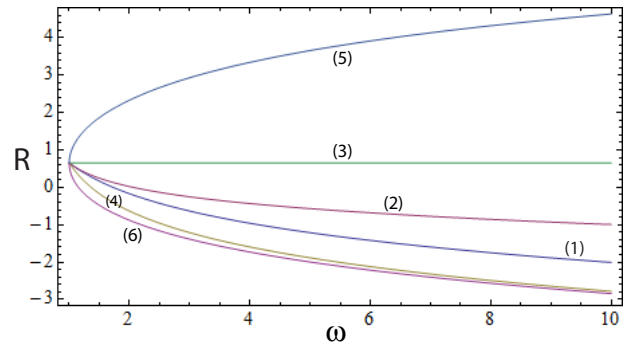


FIG. 3: (Color online) Secret-key rate R (bits) versus thermal noise ω for the various symmetric attacks (1)-(6) classified in Sec. IV and displayed in Fig. 2. Link-transmissivity is set to $\tau = 0.9$. Note that the negative EPR attack (6) is the optimal attack minimizing the rate of the protocol.

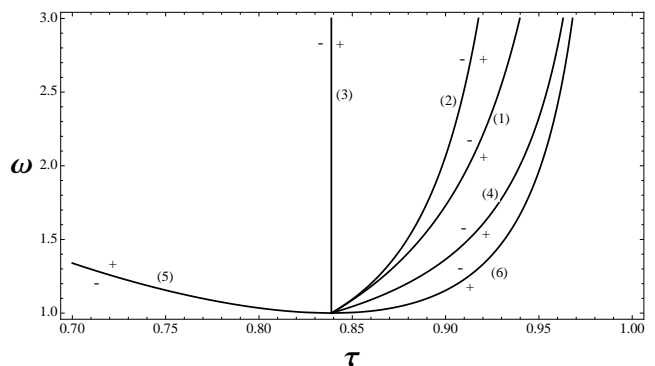


FIG. 4: (Color online) Security threshold ($R = 0$) expressed as maximum tolerable thermal noise ω versus link-transmissivity τ . We compare the various symmetric attacks (1)-(6) classified in Sec. IV and displayed in Fig. 2. The negative EPR attack (6) is the optimal corresponding to the lowest security threshold. Also note the peculiar inversion of the threshold for the positive EPR attack (5), for which the rate is positive for values of thermal noise *above* the threshold.

$\omega - 1 < g \leq \sqrt{\omega^2 - 1}$ and $g' = -g$, corresponding to the segment of points between (3) (excluded) and (5) (included). In Figs. 3 and 4, these attacks have curves which are intermediate between those of (3) and (5).

By contrast, bad entanglement refers to the entangled attacks in the top left area of Fig. 2, with $g = -g' < 0$ and having the attacks (4) and (6) as border points. This entanglement is instead bad because it injects correlations of the type $\hat{q}_{E_1} \approx -\hat{q}_{E_2}$ and $\hat{p}_{E_1} \approx \hat{p}_{E_2}$, which are opposite to those established by the Bell detection. In this case, Eve decreases the correlations between Alice's and Bob's variables, and she is able to eavesdrop more information, with the optimal strategy achieved by the negative EPR attack (6) as clear from the rates of Fig. 3 and the security thresholds of Fig. 4. The asymmetric version of this attack is optimal in case of asymmetric setups [11].

By comparing the curves (6) and (1) in Figs. 3 and 4, we clearly see the substantial advantage given by this

optimal attack with respect to the standard collective attack based on independent entangling cloners. Analytically, the minimum key rate associated with the optimal attack is given by

$$R_{\min} = h\left(\frac{\tau + 2\lambda_{\text{opt}}}{\tau}\right) + \log_2\left[\frac{\tau^2}{e^2\lambda_{\text{opt}}(\tau + \lambda_{\text{opt}})}\right], \quad (22)$$

with $\lambda_{\text{opt}} = (1 - \tau)(\omega + \sqrt{\omega^2 - 1})$. One can easily check this is numerically much less than the rate of the collective attack

$$R_{\text{coll}} = h\left[\frac{\tau + 2(1 - \tau)\omega}{\tau}\right] + \log_2\left\{\frac{\tau^2}{e^2(1 - \tau)[\tau + (1 - \tau)\omega]\omega}\right\}. \quad (23)$$

Thus, the security analysis which is valid for one-way continuous-variable QKD protocols [13], and based on the study of collective (single-mode) entangling-cloner attacks, cannot be applied to our relay-based protocol. For this reason, the studies provided by Refs. [16, 17] are incomplete and cannot prove the unconditional security of the relay-based (measurement-device independent) QKD with continuous variables.

V. CONCLUSIONS

In conclusion, we have provided a detailed analysis of the relay-based QKD protocol of Ref. [11], considering a completely symmetric setup under the action of symmetric attacks. Despite the fact that this particular case does not represent the optimal configuration of the scheme, still it is important for its potential implementation in network scenarios. Furthermore, the symmetry conditions allow us to greatly simplify the cryptanalysis and derive simple analytical results.

Thanks to this approach, we have been able to provide a very detailed classification of the symmetric attacks against the protocol, characterizing the different possible strategies in terms of their correlation properties. At fixed transmissivity and thermal noise, we have identified the optimal symmetric attack which corresponds to a coherent attack where the ancillas are maximally entangled with a specific type of EPR correlations (negative EPR attack). In particular, this attack greatly outperforms the standard collective attack based on independent entangling-cloners, which is therefore unsuitable for assessing the security of this kind of protocol (contrary to the claims of other analysis [16, 17]). This also confirms the results of Ref. [11] which were given in the general case of asymmetric setups.

Finally our work clarifies the crucial role of quantum correlations in assessing the security of QKD protocols which are based on untrusted relays. Further studies may include the extension of this protocol to thermal-QKD [21, 30, 31], with the aim of using different wave-

lengths of the electromagnetic field, e.g., in mixed technology platforms using both optical/infrared and microwave carriers.

Acknowledgments

This work was funded by a Leverhulme Trust research fellowship, the EPSRC via ‘HIPERCOM’ (grant no. EP/J00796X/1), ‘qDATA’ (grant no. EP/L011298/1) and the UK Quantum Technology Hub for Quantum Communications Technologies (Grant no. EP/M013472/1).

Appendix A: Extension to experimental imperfections

In this appendix we analyze the role of experimental imperfections computing the key-rates and the security thresholds in the presence of Bell detectors with non-ideal quantum efficiencies. We also study finite-size effects connected with finite Gaussian modulations [13], and the role played by the non-ideal efficiency of the classical reconciliation codes [32]. We show that, also in the presence of realistic experimental limitations, the optimal eavesdropping is given by the two-mode coherent “negative-EPR attack”.

1. Post-relay covariance matrix for non-ideal Bell detectors

We generalize Eq.(6) to include detectors’ efficiencies by placing two beam splitters with transmissivities η and η' , as illustrated in Fig. 5. To preserve the purity of the global (Alice-Bob-Eve) state, the non-detected signals are sent to Eve’s quantum memory (this is the assumption to make in the worst-case scenario, since the relay is untrusted and Eve can control the loss of the detectors).

We follow the general approach given in Ref. [19]. We write the total CM in the block form

$$\mathbf{V} = \begin{pmatrix} \mathbf{V}_{ab} & \mathbf{C} \\ \mathbf{C}^T & \mathbf{B} \end{pmatrix}, \quad (A1)$$

where the block

$$\mathbf{B} = \begin{pmatrix} \mathbf{B}_1 & \mathbf{D} \\ \mathbf{D}^T & \mathbf{B}_2 \end{pmatrix}, \quad (A2)$$

describes the modes sent to the relay, A' and B' . These are processed by the balanced beam splitter and then measured. In our case it is easy to verify [11, 19] that the blocks $\mathbf{B}_1, \mathbf{B}_2$ and \mathbf{D} take the following expressions

$$\mathbf{B}_1 = \mathbf{B}_2 = [\tau\mu + (1 - \tau)\omega]\mathbf{I}, \quad (A3)$$

$$\mathbf{D} = (1 - \tau)\mathbf{G}, \quad (A4)$$

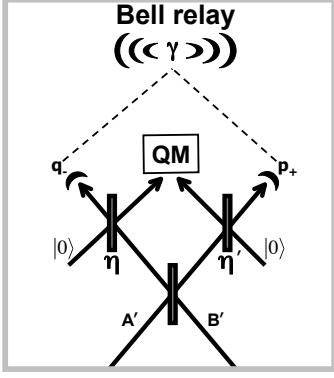


FIG. 5: (Color online) Untrusted relay with inefficient detectors. Two additional beam splitters, with transmissivities (η, η') are placed in front of the ideal detectors. One output from each beam splitter is sent to the detectors for measurements. The other outputs are sent to Eve's quantum memory.

where $\mathbf{I} = \text{diag}(1, 1)$ and $\mathbf{G} = \text{diag}(g, g')$.

In Eq. (A1) the sub-matrix \mathbf{V}_{ab} describes the joint quantum state of remote modes a and b , while the block $\mathbf{C} = (\mathbf{C}_1 \mathbf{C}_2)$ is a rectangular matrix accounting for the correlations between the remote modes and the transmitted ones, i.e., A' and B' . In particular, we compute

$$\mathbf{C}_1 = \begin{pmatrix} \sqrt{\tau(\mu^2 - 1)}\mathbf{Z} \\ \mathbf{0} \end{pmatrix}, \quad \mathbf{C}_2 = \begin{pmatrix} \mathbf{0} \\ \sqrt{\tau(\mu^2 - 1)}\mathbf{Z} \end{pmatrix}. \quad (\text{A5})$$

Applying Eq. (74) from Ref. [19] to Eq. (A1), we obtain Alice and Bob's CM conditioned to the relay Bell measurement. This is given by

$$\mathbf{V}_{ab|\gamma} = \mathbf{V}_{ab} - \frac{1}{2 \det \gamma(\eta, \eta')} \sum_{i,j=1,2} \mathbf{C}_i \left(\mathbf{X}_i^T \gamma(\eta, \eta') \mathbf{X}_j \right) \mathbf{C}_j^T, \quad (\text{A6})$$

where

$$\mathbf{X}_1 = \begin{pmatrix} 1 & 1 \\ 1 & 1 \end{pmatrix}, \quad \mathbf{X}_2 = \begin{pmatrix} 1 & 1 \\ -1 & 1 \end{pmatrix}. \quad (\text{A7})$$

Here the quantum efficiencies of the detectors, simulated by the beam splitter transmissivities η and η' , are contained in the symmetric matrix

$$\gamma(\eta, \eta') = \begin{pmatrix} \gamma_1(\eta) & \gamma_3 \\ \gamma_3 & \gamma_2(\eta') \end{pmatrix}. \quad (\text{A8})$$

In the case of a Bell detection the matrix $\gamma(\eta, \eta')$ can explicitly be computed, according to Eqs. (54-59) of Ref. [19]. In particular, its entries take the form

$$\begin{aligned} \gamma_1(\eta) &= \gamma_1 + \frac{1 - \eta}{\eta}, \\ \gamma_2(\eta') &= \gamma_2 + \frac{1 - \eta'}{\eta'}, \\ \gamma_3 &= 0 \end{aligned} \quad (\text{A9})$$

where $\gamma_1 = \tau\mu + (1 - \tau)(\omega - g)$ and $\gamma_2 = \tau\mu + (1 - \tau)(\omega + g')$ are easily obtained from Eq. (A3) and (A4), using the formulas of Ref. [19].

After simple algebra we derive the post-relay CM inclusive of the quantum efficiencies

$$\mathbf{V}_{ab|\gamma} = \begin{pmatrix} \mu \mathbf{I} & \mathbf{0} \\ \mathbf{0} & \mu \mathbf{I} \end{pmatrix} - \frac{\tau(\mu^2 - 1)}{2} \times \begin{pmatrix} \frac{1}{\gamma_1(\eta)} & -\frac{1}{\gamma_1(\eta)} & & \\ -\frac{1}{\gamma_1(\eta)} & \frac{1}{\gamma_2(\eta')} & \frac{1}{\gamma_1(\eta)} & \frac{1}{\gamma_2(\eta')} \\ & \frac{1}{\gamma_2(\eta')} & \frac{1}{\gamma_1(\eta)} & \frac{1}{\gamma_2(\eta')} \end{pmatrix}.$$

This CM can be rewritten in the form

$$\mathbf{V}_{ab|\gamma} = \begin{pmatrix} \mu \mathbf{I} & \mathbf{0} \\ \mathbf{0} & \mu \mathbf{I} \end{pmatrix} - \frac{\tau(\mu^2 - 1)}{2} \times \begin{pmatrix} \frac{1}{\tau\mu + \lambda(\eta)} & -\frac{1}{\tau\mu + \lambda(\eta)} & & \\ -\frac{1}{\tau\mu + \lambda(\eta)} & \frac{1}{\tau\mu + \lambda'(\eta')} & \frac{1}{\tau\mu + \lambda(\eta)} & \frac{1}{\tau\mu + \lambda'(\eta')} \\ & \frac{1}{\tau\mu + \lambda'(\eta')} & \frac{1}{\tau\mu + \lambda(\eta)} & \frac{1}{\tau\mu + \lambda'(\eta')} \end{pmatrix}, \quad (\text{A10})$$

where

$$\begin{cases} \lambda(\eta) = (\omega - g)(1 - \tau) + \frac{1 - \eta}{\eta}, \\ \lambda'(\eta') = (\omega + g')(1 - \tau) + \frac{1 - \eta'}{\eta'}. \end{cases} \quad (\text{A11})$$

Note that Eq. (A10) could have been computed directly from Eq. (6) by applying the transformations [34]

$$\lambda \rightarrow \lambda(\eta), \quad \lambda' \rightarrow \lambda'(\eta'). \quad (\text{A12})$$

2. Asymptotic generalized key-rate

From the previous CM we can write the sub-matrix describing Bob's mode

$$\mathbf{V}_{b|\gamma} = \begin{pmatrix} \mu - \frac{\tau(\mu^2 - 1)}{2[\tau\mu + \lambda(\eta)]} & \\ & \frac{\tau(\mu^2 - 1)}{2[\tau\mu + \lambda'(\eta')]} \end{pmatrix}. \quad (\text{A13})$$

Then, by applying Eq. (13) to the generalized CM of Eq. (A10), we derive the doubly-conditional CM of Bob, conditioned to both relay's and Alice's detections, i.e.,

$$\mathbf{V}_{b|\gamma\alpha}(\eta, \eta') = \begin{pmatrix} \mu - \frac{\tau(\mu^2 - 1)}{[\tau(\mu + 1) + 2\lambda(\eta)]} & \\ & \mu - \frac{\tau(\mu^2 - 1)}{[\tau(\mu + 1) + 2\lambda'(\eta')]} \end{pmatrix}. \quad (\text{A14})$$

We can now derive the symplectic spectra of the CMs of Eq. (A10) and (A14). We find simple analytical expressions in the limit of large modulation. For $\mathbf{V}_{ab|\gamma}$ we have the symplectic eigenvalues $\nu_1(\eta)$ and $\nu_2(\eta')$, while for $\mathbf{V}_{b|\gamma\alpha}$ we have $\nu(\eta, \eta')$. These eigenvalues can be obtained by applying the transformations of Eq. (A12) to the Eqs. (8) and (15).

Using these spectra, we can compute the corresponding total and conditional von Neumann entropies and therefore the Holevo bound. In the limit of large modulation, Eve's Holevo information becomes

$$I_{E|\gamma}(\eta, \eta') = \log_2 \frac{e^2 \sqrt{\lambda(\eta)\lambda'(\eta')}\mu}{4\tau} - h \left[\frac{\sqrt{[\tau + 2\lambda(\eta)][\tau + 2\lambda'(\eta')]} }{\tau} \right], \quad (\text{A15})$$

which extends Eq. (16) to arbitrary efficiencies η and η' .

Similarly, we can extend the formula for Alice and Bob's mutual information, which here becomes

$$I_{AB|\gamma}(\eta, \eta') = \log_2 \frac{\tau\mu}{4\sqrt{[\tau + \lambda(\eta)][\tau + \lambda'(\eta')]}}, \quad (\text{A16})$$

for large modulation. Combining the previous results, we derive the asymptotic key-rate in the presence of detector inefficiencies

$$R_{sym}(\eta, \eta') = \log_2 \left[\frac{\tau^2}{e^2 \sqrt{\lambda(\eta)\lambda'(\eta')[\tau + \lambda(\eta)][\tau + \lambda'(\eta')]} } \right] + h \left[\frac{\sqrt{[\tau + 2\lambda(\eta)][\tau + 2\lambda'(\eta')]} }{\tau} \right], \quad (\text{A17})$$

which clearly extends the formula given in Eq. (18).

3. Role of the imperfections on key-rate, security thresholds and achievable distances

In this section we study in detail the combined role of the various experimental limitations and imperfections, confirming the main findings presented in the main body of this paper. We compute the key-rate and the security thresholds considering not only the realistic quantum efficiency of the detectors, but also the use of a finite Gaussian modulation and the non-ideal reconciliation efficiency provided by realistic codes for error correction and privacy amplification.

a. Secret key rate

In order to extract a secret key, the honest parties must process their correlated data in stages of perform error correction and privacy amplification. This data processing is today implemented with a limited efficiency $\beta \leq 1$, for instance $\beta \simeq 0.95 \div 0.97$ [32, 33]. To include this limitation, we have to multiply Alice and Bob's mutual information by β , and consider the realistic key-rate [13]

$$R(\beta, \mu, \tau, \omega, g, g', \eta, \eta') = \beta I_{AB|\gamma} - I_{E|\gamma}, \quad (\text{A18})$$

where $I_{AB|\gamma}$ and $I_{E|\gamma}$ are now computed considering finite modulation μ besides non-ideal detector efficiencies

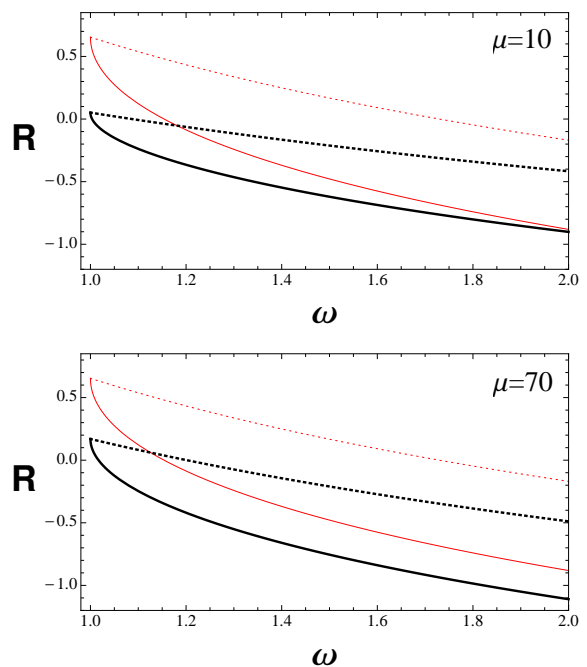


FIG. 6: (Color online) The key-rate R (bits) is plotted versus thermal noise ω for $\mu = 10$ (SNU) (top-panel) and $\mu = 70$ (bottom-panel). Other parameters are $\tau = 0.9$, $\beta = 0.95$ and $\eta = \eta' = 0.98$. We compare two eavesdropping strategies: The collective one-mode entangling cloner attack $g' = g = 0$ (dotted black line) and the two-mode “negative EPR” attack $g = -g' = -\sqrt{\omega^2 - 1}$ (continuous black line). We see that the key-rate of the two-mode attack is always lower than that of the one-mode attack. For comparison, we have also plotted the performances in the case of ideal reconciliation ($\beta = 1$), ideal detectors ($\eta = \eta' = 1$) and large modulation ($\mu \gg 1$). These ideal performances are represented by the red curves, dotted for the one-mode attack and continuous for the two-mode attack.

η and η' (clearly these quantities must tend to Eqs. (A15) and (A16) in the limit of large modulation).

In general, the mutual information can be computed from the formula $I_{AB|\gamma} = \frac{1}{2} \log_2 \Sigma$, where Σ is defined in Ref. [11]. Eve's Holevo information can be computed using the formula of the von Neumann entropy $S = \sum_x h(x)$, with $h(x)$ defined in Eq. (9) and applied to the numerical symplectic eigenvalues of the CMs given in Eqs. (A10) and (A14). In Fig. 6, we plot the key-rate of Eq. (A18) as a function of the thermal noise ω for two values of the Gaussian modulation $\mu = 10$ (top) and $\mu = 70$ (bottom) vacuum shot noise unit (SNU), and choosing $\tau = 0.9$, $\eta = \eta' = 0.98$ and $\beta = 0.95$. We see that the key-rate of a negative EPR attack is clearly lower than that of a collective one-mode attack. This behavior is generic by varying the previous parameters.

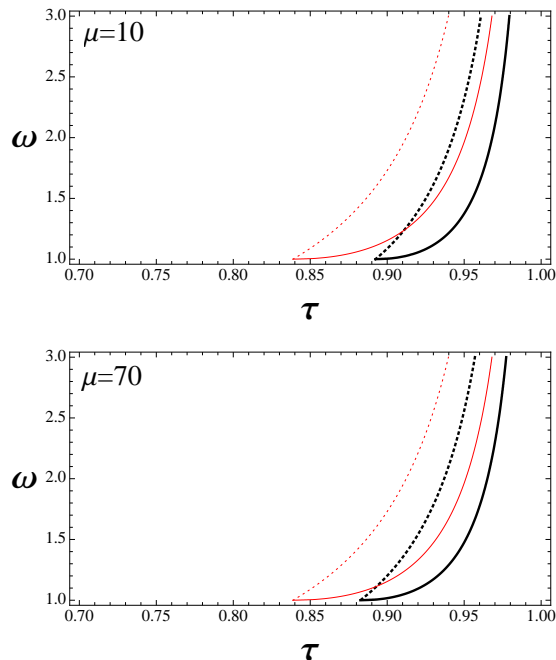


FIG. 7: (Color online) We plot the security threshold $\omega = \omega(\tau)$ for $\mu = 10$ (top panel) and $\mu = 70$ (bottom panel). Other parameters are $\beta = 0.95$ and $\eta = \eta' = 0.98$. We compare the two-mode negative EPR attack (continuous black lines) and the one-mode entangling cloner attack (dotted black lines). Red curves refer to the ideal case $\beta = \eta = \eta' = 1$ and $\mu \gg 1$.

b. Security thresholds and achievable distances

Here we study the impact of the experimental limitations on the security thresholds, comparing the two-mode optimal attack with one-mode collective attack. The security threshold is obtained by solving the equation

$$R(\beta, \mu, \tau, \omega, g, g', \eta, \eta') = 0. \quad (\text{A19})$$

In this equation, we fix the values of the Gaussian modulation ($\mu = 10$ or 70), the reconciliation efficiency ($\beta = 0.95$), and the quantum efficiencies $\eta = \eta' = 0.98$. Then, for each attack, we can write the security threshold as $\omega = \omega(\tau)$. The comparison is provided in Fig. 7, where we see that the threshold of the optimal two-mode attack is always lower than the threshold of the one-mode collective attack.

The previous analysis can be performed by expressing the transmissivity in term of distances. In fact, we may consider $\tau = 10^{-\frac{0.2}{10}d}$, where d is the distance in km, assuming the standard loss rate in fibre of 0.2dB/Km. The achievable distances are shown in Fig. 8. We see that moving from the ideal conditions (red curves, with $\beta = \eta = \eta' = 1$ and $\mu \gg 1$) the performances deteriorate. All others curves are obtained for realistic reconciliation efficiencies $\beta = 0.95$, and detectors efficiencies $\eta = \eta' = 0.98$. The top panel compares the ideal thresholds with the case $\mu = 70$ (black), while in the bottom panel we show the degradation of the performances

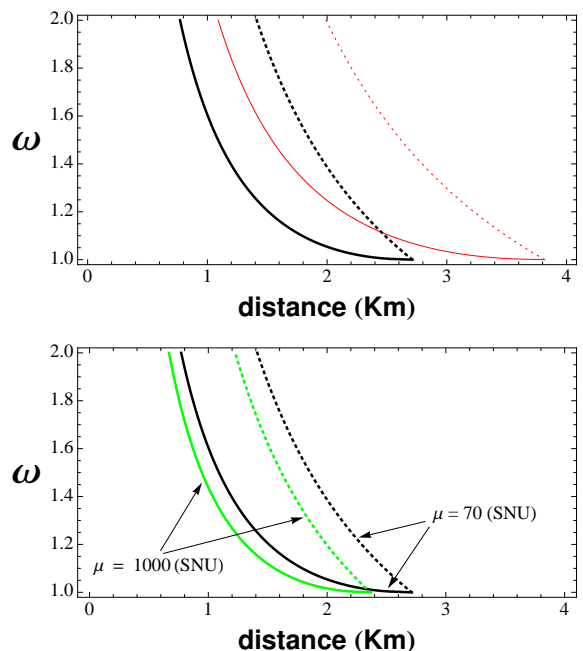


FIG. 8: (Color online) This figure shows the security thresholds as $\omega = \omega(d)$, where d is the distance in km, assuming the loss rate of 0.2 dB/Km. As in previous figures we compare the two-mode negative EPR attack (solid lines) with the one-mode entangling-cloner attack (dotted lines). In the top panel, the red curves refer to the ideal conditions $\beta = \eta = \eta' = 1$ and $\mu \gg 1$. The black curves refer to the non ideal case $\beta = 0.95$, $\eta = \eta' = 0.98$ and $\mu = 70$ (SNU). The bottom panel shows the degradation of the performance as we increase the modulation from $\mu = 70$ (black curves) to $\mu = 1000$ (green curves), for $\beta = 0.95$, $\eta = \eta' = 0.98$.

while increasing the modulation from $\mu = 70$ (black) to $\mu = 1000$ (green).

It is interesting to note the effect of the reconciliation efficiency on the optimal modulation variance. For values of $\beta < 1$, the optimal modulation is not infinite. In fact, for the realistic value considered here, $\beta = 0.95$, we have a range of finite modulations $30 \lesssim \mu \lesssim 70$, for which the performances are improved.

c. Discussion

Here we summarize some important aspects emerged from this further analysis. First, we have shown that positive key-rates are still achievable over the range of metropolitan distances in the presence of various experimental limitations. Second, the negative-EPR attack, already identified to be the optimal attack in the ideal case (see main text) continues to be the most powerful eavesdropping strategy also considering realistic experimental conditions, i.e., finite modulation, non-ideal reconciliation and non-ideal detectors. Third, the degradation of the performances of the protocol does not come from the finite modulation (e.g., we checked that values

as low as $\mu = 10$ are still acceptable) but mainly from the quantum efficiencies of the detectors, η and η' , and

the reconciliation efficiency β of the classical codes.

-
- [1] B. Schneier, Applied Cryptography (John Wiley & Sons, New York, 1996) p.23.
- [2] N. Gisin, G. Ribordy, W. Tittel, and H. Zbinden, Rev. Mod. Phys. **74**, 145 (2002).
- [3] SECOQC, 2007, <http://www.secoqc.net>
- [4] M. Peev *et al.*, New J. Phys. **11**, 075001 (2009).
- [5] Tokyo QKD network 2010, www.uqcc.org/QKDnetwork.
- [6] J. H. Saltzer, D. P. Reed, and D. D. Clark, *Proceedings of the Second International Conference on Distributed Computing Systems* (Paris, France, April 8-10, 1981).
- [7] P. Baran, IEEE Trans. on Comm. **12**, pp. 1-9 (1964).
- [8] S. L. Braunstein, and S. Pirandola, Phys. Rev. Lett. **108**, 130502 (2012).
- [9] A. Rubenok, J. A. Slater, P. Chan, I. Lucio-Martinez, and W. Tittel, Phys. Rev. Lett. **111**, 130501 (2013).
- [10] T. Ferreira da Silva, D. Vitoreti, G. B. Xavier, G. C. do Amaral, G. P. Temporão, and J. P. von der Weid, Phys. Rev. A **88**, 052303 (2013).
- [11] S. Pirandola, C. Ottaviani, G. Spedalieri, C. Weedbrook, S.L. Braunstein, S. Lloyd, T. Gehering, C.S. Jacobsen and U.L. Andersen, arXiv.1312.4104.
- [12] S. L. Braunstein and P. van Loock, Rev. Mod. Phys. **77**, 513 (2005).
- [13] C. Weedbrook, S. Pirandola, R. Garcia-Patron, N. J. Cerf, T. C. Ralph, J. H. Shapiro, and S. Lloyd, Rev. Mod. Phys. **84**, 621 (2012).
- [14] R. García-Patrón and N.J. Cerf, Phys. Rev. Lett. **97**, 190503 (2006).
- [15] M. Navascues, F. Grosshans, A. Acin, Phys. Rev. Lett. **97**, 190502 (2006).
- [16] Z. Li, Y-C. Zhang, F. Xu, X. Peng, and H. Guo, Phys. Rev. A **89**, 052301 (2014).
- [17] X-C. Ma, S-H. Sun, M-S. Jiang, M. Gui, and L-M. Liang, Phys. Rev. A **89**, 042335 (2014).
- [18] Note that Ref. [17] computed the rate of the protocol at fixed transmissivity τ and thermal noise ω , since they fixed both τ and $\varepsilon = (\omega - 1)(1 - \tau)/\tau$. However, while the latter formula provides the excess noise for standard one-way protocols [13] it does not for the considered relay-based protocol (see Ref. [11] for the correct definition of excess noise in this more complex case).
- [19] G. Spedalieri, C. Ottaviani, and S. Pirandola, Open Syst. Inf. Dyn. **20**, 1350011 (2013).
- [20] S. Pirandola, S. Mancini, S. Lloyd, and S. L. Braunstein, Nature Phys. **4**, 726 (2008).
- [21] C. Weedbrook, C. Ottaviani, and S. Pirandola, Phys. Rev. A **89**, 012309 (2014).
- [22] M.A. Nielsen and I. L. Chuang, *Quantum Computation and Quantum Information* (Cambridge University Press, Cambridge, 2000).
- [23] M. M. Wilde, *From Classical to Quantum Shannon Theory* (Cambridge University Press, Cambridge, 2013).
- [24] G. Giedke and J.I. Cirac, Phys. Rev. A **66**, 032316 (2002).
- [25] R. Renner, Nature Phys. **3**, 645 (2007).
- [26] R. Renner, J.I. Cirac, Phys. Rev. Lett. **102**, 110504 (2009).
- [27] S. Pirandola, S. L. Braunstein, and S. Lloyd, Phys. Rev. Lett. **101**, 200504 (2008).
- [28] S. Pirandola, A. Serafini, and S. Lloyd, Phys. Rev. A **79**, 052327 (2009).
- [29] S. Pirandola, New J. Phys. **15**, 113046 (2013).
- [30] C. Weedbrook, S. Pirandola, S. Lloyd, and T.C. Ralph, Phys. Rev. Lett. **105**, 110501 (2010).
- [31] C. Weedbrook, S. Pirandola, and T.C. Ralph, Phys. Rev. A **86**, 022318 (2012).
- [32] Paul Jouguet, Sébastien Kunz-Jacques, Anthony Leverrier, Phys. rev. A **84**, 062317 (2011).
- [33] P. Jouguet, S. Kunz-Jacques, A. Leverrier, P. Grangier, E. Diamanti, Nat. Photonics **7**, 378 (2013).
- [34] Note that, in the presence of a pure-loss attack ($\omega = 1$ and $g = g' = 0$), the non-unit quantum efficiencies of the detectors can be included in the loss of the channels. For simplicity, for $\eta = \eta'$ we can write
- $$\frac{\tau}{\tau\mu + \lambda(\eta)} = \frac{\tau\eta}{\tau\eta\mu + 1 - \tau\eta}$$
- which is equivalent to consider $\tau\eta$ in the CM of Eq. (6).